



Ion-irradiation-induced ferromagnetism in undoped ZnO thin films [☆]

Siddhartha Mal ^{a,*}, Sudhakar Nori ^a, J. Narayan ^a, J.T. Prater ^b, D.K. Avasthi ^c

^a Department of Materials Science and Engineering, North Carolina State University, Raleigh, NC 27695, USA

^b Materials Science Division, Army Research Office, Research Triangle Park, NC 27709, USA

^c Materials Science Group, Inter University Accelerator Centre, Aruna Asaf Ali Marg, PO Box 10502, New Delhi 110 067, India

Abstract

We have introduced defects in ZnO epitaxial thin films by swift heavy $^{107}\text{Ag}^{9+}$ ion irradiation and investigated systematically their magnetic, electrical and optical properties. Oxygen annealed ZnO films are epitaxial single crystals that exhibit no long-range magnetic order. However, in this paper it is shown that room-temperature ferromagnetism (RTFM) can be introduced in a controlled manner in these films using ion irradiation and that the magnetization increases with ion dose. This qualitatively agrees with earlier studies which showed that RTFM could be induced in ZnO films through either vacuum thermal annealing or pulsed laser annealing below energy densities that lead to melting. Raman studies of the ion irradiated samples revealed dramatic changes in the vibration modes that correlated with increases in the carrier concentration, indicative of lattice disorder and defect creation. We compare these results with those observed in laser irradiated and vacuum annealed samples, and then discuss these findings in the context of defects and defect complexes created during the high-energy heavy ion irradiation process. We propose a unified mechanism to explain RTFM and n-type conductivity enhancements during irradiation, and laser and vacuum annealing.

© 2012 Published by Elsevier Ltd. on behalf of Acta Materialia Inc.

Keywords: Zinc oxide; Thin films; Pulsed laser deposition; Magnetic semiconductors; Raman spectra

1. Introduction

Recently, room temperature d^0 ferromagnetism (RTFM) has been widely reported in different ZnO nanostructures lacking any intentional magnetic doping [1–3]. This unconventional ferromagnetism has also been found in other undoped metal oxides, such as HfO_2 , TiO_2 , SnO_2 and In_2O_3 [4,5]. The origin of ferromagnetism and the mechanism which provides some degree of three-dimensional (3-D) ferromagnetic ordering in these oxides is not clear at this moment. However there is a growing consensus that the ferromagnetism in undoped ZnO is directly linked to material imperfections, including poor crystalline quality, strain, grain boundaries and intrinsic defects, namely oxygen vacancies (V_{O}), zinc vacancies (V_{Zn}) and

zinc interstitials (I_{Zn}). To date, RTFM has been induced in undoped ZnO powder by application of mechanical deformation [6], and by laser irradiation or vacuum annealing of the films [7,8].

It is envisaged that RTFM and changes in n-type conductivity are caused by defects introduced during these treatments. Recent ab initio calculations have suggested that the magnetic moment may arise from the unpaired 2p electrons at the O sites surrounding the zinc vacancy with each nearest-neighbor O atom carrying a magnetic moment ranging from 0.49 to 0.74 μ_{B} [9]. The source of n-type conductivity in ZnO has been attributed to oxygen vacancy–hydrogen [10], and oxygen vacancy and zinc interstitial ($V_{\text{O}}\text{--}I_{\text{Zn}}$) complexes [11].

In this paper, we have introduced defects uniformly throughout the thickness of the films using swift heavy ion (SHI) irradiation. Here the ion energy of $^{107}\text{Ag}^{9+}$ is 300 MeV, for which electronic stopping (20 keV nm^{−1}) dominates over the nuclear stopping (0.03 keV nm^{−1}). Under these conditions, the ion energy losses are primarily

[☆] This article was presented at the symposium held in honor of Professor Jagdish Narayan, the recipient of the Acta Materialia Gold Medal Award.

* Corresponding author.

E-mail address: smal@ncsu.edu (S. Mal).

Report Documentation Page				Form Approved OMB No. 0704-0188	
Public reporting burden for the collection of information is estimated to average 1 hour per response, including the time for reviewing instructions, searching existing data sources, gathering and maintaining the data needed, and completing and reviewing the collection of information. Send comments regarding this burden estimate or any other aspect of this collection of information, including suggestions for reducing this burden, to Washington Headquarters Services, Directorate for Information Operations and Reports, 1215 Jefferson Davis Highway, Suite 1204, Arlington VA 22202-4302. Respondents should be aware that notwithstanding any other provision of law, no person shall be subject to a penalty for failing to comply with a collection of information if it does not display a currently valid OMB control number.					
1. REPORT DATE 2013		2. REPORT TYPE		3. DATES COVERED 00-00-2013 to 00-00-2013	
4. TITLE AND SUBTITLE Ion-irradiation-induced ferromagnetism in undoped ZnO thin films				5a. CONTRACT NUMBER	
				5b. GRANT NUMBER	
				5c. PROGRAM ELEMENT NUMBER	
6. AUTHOR(S)				5d. PROJECT NUMBER	
				5e. TASK NUMBER	
				5f. WORK UNIT NUMBER	
7. PERFORMING ORGANIZATION NAME(S) AND ADDRESS(ES) Army Research Office, Materials Science Division, Research Triangle Park, NC, 27709				8. PERFORMING ORGANIZATION REPORT NUMBER	
9. SPONSORING/MONITORING AGENCY NAME(S) AND ADDRESS(ES)				10. SPONSOR/MONITOR'S ACRONYM(S)	
				11. SPONSOR/MONITOR'S REPORT NUMBER(S)	
12. DISTRIBUTION/AVAILABILITY STATEMENT Approved for public release; distribution unlimited					
13. SUPPLEMENTARY NOTES Preprint Acta Materialia xxx (2013)					
14. ABSTRACT					
15. SUBJECT TERMS					
16. SECURITY CLASSIFICATION OF:			17. LIMITATION OF ABSTRACT Same as Report (SAR)	18. NUMBER OF PAGES 7	19a. NAME OF RESPONSIBLE PERSON
a. REPORT unclassified	b. ABSTRACT unclassified	c. THIS PAGE unclassified			

due to electronic excitations that couple with phonons to dissipate their energy as heat with relaxation times on the order of picoseconds. We compare these results with previous pulsed laser annealing and vacuum annealing studies, which are expected to introduce nonhomogeneous defect profiles, and find that they are mutually consistent with a defect-induced RTFM mechanism.

2. Experimental approach

ZnO thin films $\sim 1\ \mu\text{m}$ thick have been deposited onto single crystal *c*-plane sapphire substrates in a pulsed laser deposition system using a KrF excimer laser ($\lambda = 248\ \text{nm}$, $\tau = 25\ \text{ns}$) with a pulse energy density of $3\text{--}4\ \text{J cm}^{-2}$ at a repetition rate of $10\ \text{Hz}$. The films were grown at $550\ ^\circ\text{C}$ and under an oxygen partial pressure of $10^{-5}\ \text{Torr}$. Oxygen annealing was then performed at $700\ ^\circ\text{C}$ for $1\ \text{h}$ under $760\ \text{Torr}$. Finally, the epitaxial ZnO thin films were irradiated using $300\ \text{MeV}\ ^{107}\text{Ag}^{9+}$ ions of 10^{12} and $10^{13}\ \text{ions cm}^{-2}$ dose at the Inter University Accelerator Centre Facility in New Delhi, India. Details of the growth and characterization have been reported previously [8]. Optical transmission measurements were made using a Hitachi Spectrophotometer. The magnetization measurements were performed using an alternate gradient magnetometer (AGM) (Princeton Applied Research). The resolution of the AGM is on the order of $1.0\ \text{nano-emu}$, which is approximately three orders of magnitude more sensitive to the magnetic moments of the samples that were measured in the current study. As a matter of fact the authors, in their previous investigations, did carry out the field- as well as the temperature-dependent magnetization measurements extensively on doped and undoped ZnO thin films using both (i) a vibrating sample magnetometer (VSM) in conjunction with a physical property measurement system (PPMS) and SQUID magnetometers (Quantum Design). The measured magnetic moments for Co-doped ZnO and undoped ZnO films are in range of 5.0×10^{-5} – $5.0 \times 10^{-6}\ \text{emu cm}^{-3}$ after subtracting the diamagnetic contribution arising due to the sapphire substrates carefully and the same were published previously [7,8].

3. Results and discussion

During ion irradiation, the deposition of a large amount of energy to the lattice occurs on the order of picoseconds through both nuclear (S_n) and electronic (S_e) energy loss mechanisms. The S_n for $300\ \text{MeV}\ ^{107}\text{Ag}^{9+}$ ions in ZnO is $0.03\ \text{keV nm}^{-1}$, while the S_e is $20\ \text{keV nm}^{-1}$, as calculated from SRIM-2008 calculations [12]. Fig. 1 shows that the nuclear stopping mechanism dominates only at lower energy ($<3\ \text{MeV}$), whereas the electronic stopping mechanism dominates at the higher energies used in this study. The nuclear stopping, which is an elastic process, creates vacancies and interstitials through the transfer of energy to the target lattice that results in atomic displacements in the form of Frankel defects in the form of zinc vacancy

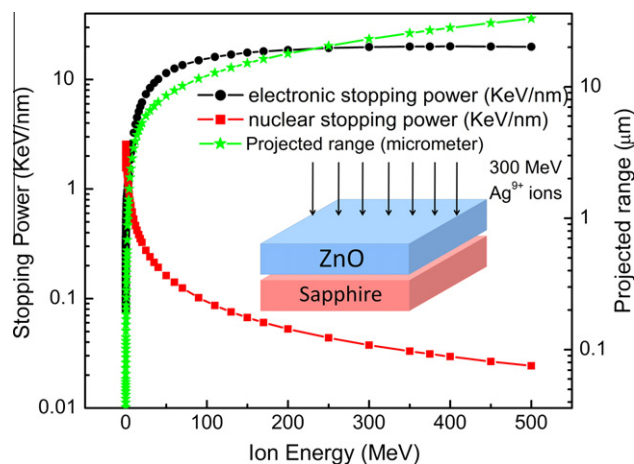


Fig. 1. Nuclear and electronic stopping powers and projected range as a function of energy of $^{107}\text{Ag}^{9+}$ ions. The inset shows the schematic of the thin film heterostructure and normal incidence of ions.

and zinc interstitial ($V_{\text{Zn}}\text{--}I_{\text{Zn}}$) and oxygen vacancy and interstitial ($V_{\text{O}}\text{--}I_{\text{O}}$) pairs. On the other hand, the inelastic electronic stopping process transfers a large amount of energy to the ZnO lattice through electron–photon interactions. According to the thermal spike model, the temperature in a narrow cylindrical zone of $\sim 10\ \text{nm}$ around the ion tracks increases to temperatures in excess of the melting point of ZnO [13]. The rise in temperature is followed by a rapid thermal quenching ($\sim 10^{14}\ \text{K s}^{-1}$), resulting in non-equilibrium thermodynamic processes that can create point defects like oxygen and zinc vacancies and interstitials. The electronic excitations are also known to cause breaking of chemical bonds due to the collisions between ions and electrons [12,13] at high ion fluencies such as those used in our study (10^{12} and $10^{13}\ \text{ions cm}^{-2}$). It can be seen from Fig. 1 that the projected range of penetration for the swift heavy ions is much more than the thickness of the ZnO films. Thus, the effect of the ion irradiation is expected to be uniform across the whole thickness of the film and directly proportional to the dose. This, in fact, is the unique distinction of ion irradiation over other processing treatments, e.g. thermal annealing or laser irradiation, where conditions at the surfaces could be quite different from the bulk of the film [14,15].

Fig. 2 shows X-ray diffraction characterization (2θ -intensity scan) of oxygen annealed and ion irradiated ZnO films at different doses of 10^{12} and $10^{13}\ \text{ions cm}^{-2}$. The XRD pattern shows that the films are highly textured with a *c*-axis preferred orientation. The epitaxial nature of these films was established by ϕ -scans and cross-section TEM as shown in Fig. 3. It can also be seen that there is no substantial change in the (002) diffraction peak position and the peak width. However, the intensity of the peak slightly decreased in the case of the sample exposed to the higher ion dose ($10^{13}\ \text{cm}^{-2}$), indicating a very slight degradation of crystalline quality upon ion irradiation. The ion tracks were not observed in the high-resolution

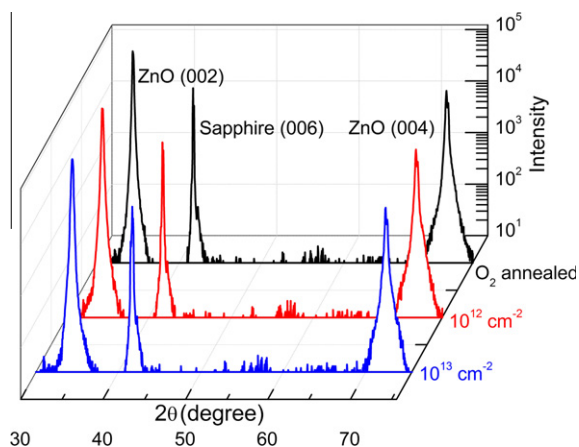


Fig. 2. X-ray diffraction patterns of oxygen annealed and oxygen annealed followed by ion irradiated films at different doses.

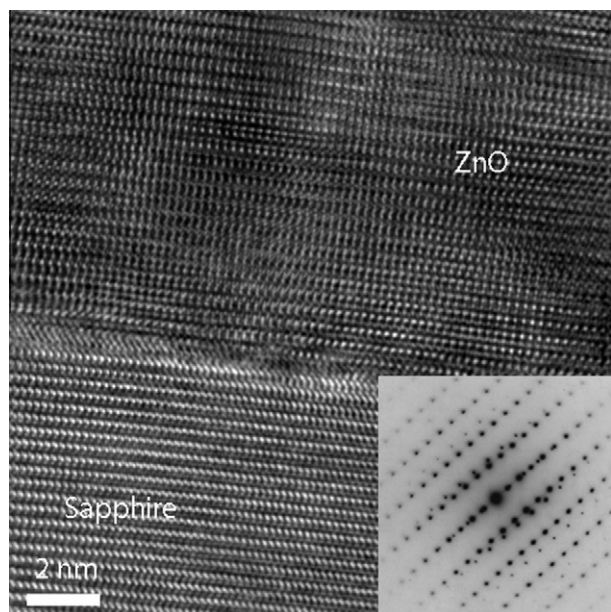


Fig. 3. High-resolution transmission electron micrograph of ZnO/sapphire interface of the sample irradiated at 10^{13} ions cm^{-2} dose. The inset shows the selected area diffraction pattern.

transmission electron micrograph, as shown in Fig. 3. The HRTEM micrograph suggests that long-range order is fully maintained and defects such as dislocations and grain boundaries are not introduced by ion irradiation. However, the point defects and their clusters are introduced which cannot be detected by HRTEM. The X-ray diffraction studies and HRTEM proved to be relatively insensitive to atomic level disorder. Therefore, Raman spectroscopy was used to gain further insight on the nature of the defects present in the samples. The wurtzite ZnO crystals belong to the space group C_{6v}^4 . Group theory predicts that for h -ZnO there are six optical phonon modes, $A_1 + 2B_1 + E_1 + 2E_2$, at the Γ -point of the Brillouin zone. The polar A_1 and E_1 modes and two nonpolar E_2 modes (E_2^{high} and E_2^{low}) are Raman active, while the B_1 modes are Raman inactive

[16]. Unpolarized Raman spectra collected under a back-scattering geometry are presented in Fig. 4. The six peaks marked by asterisks at 378, 418, 438, 451, 578 and 604 cm^{-1} originate from the sapphire substrate. In the undoped oxygen annealed (700 °C, 1 h) ZnO film only E_2^{high} and a second order phonon of $2E_2^{\text{low}}$, at ~ 432 and ~ 330 cm^{-1} respectively, are observed. The most significant features, however, of the results presented in Fig. 4 are the appearance of two silent Raman modes and a drastic change in the intensity and broadening of the E_2 peaks in films subjected to ion irradiation. The two silent Raman modes [17] centered at 260 (B_1^{low}) and 552 cm^{-1} (B_1^{high}) are attributed to disorder-activated Raman scattering processes associated with the breakdown of the translational crystal symmetry that has been induced by the presence of defects. The spectra of the irradiated films show that the intensity of the E_2^{high} mode decreases drastically upon irradiation at 10^{12} cm^{-2} fluence and disappears completely at 10^{13} cm^{-2} . In addition to the suppression of the E_2^{high} mode, it is also observed that the $2E_2^{\text{low}}$ mode centered at 330 cm^{-1} shows higher intensity in the irradiated films. Finally, it is found that the E_2^{high} mode disappears in vacuum annealed samples. The E_2^{high} and E_2^{low} modes are associated, respectively, with the oxygen and zinc sublattice [12], thus shifts in the intensity of the E_2^{high} and E_2^{low} modes would be consistent with large shifts in the concentrations of oxygen and zinc vacancies and interstitials. The $A_1(\text{LO})$ mode at 576 cm^{-1} is not clearly seen, likely because it partially overlaps with a strong sapphire E_g mode at 578 cm^{-1} . However, after Gaussian fitting for two peaks centered at 576 and 578 cm^{-1} , it can be shown that the intensity of $A_1(\text{LO})$ component increases in intensity following ion irradiation, which can be clearly seen from the broadening of the left shoulder of the peak of the irradiated films. Previously, it has been reported that the $A_1(\text{LO})$ mode is

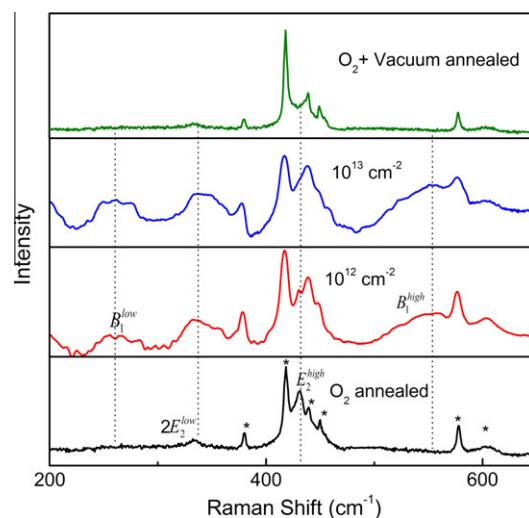


Fig. 4. Raman spectra of oxygen annealed, ion irradiated and oxygen + vacuum annealed ZnO thin films. The peaks marked by asterisks (*) originate from the sapphire substrate.

affected by the presence of defects [13]. Hence, the Raman studies confirm that the swift ion irradiation treatment, and to a much lesser extent vacuum annealing, introduces disorder into the films, which certainly includes large concentrations of intrinsic point defects associated with the oxygen and zinc sublattices.

Optical transmission spectra were measured for the oxygen annealed films (before ion irradiation) and then again after the films had been irradiated with 10^{12} and 10^{13} ions cm^{-2} . The bandgap of the alloys was determined using Tauc plots. The absorption coefficient, for direct interband transitions, is given by the relation $(\alpha h\nu) = A_0(h\nu - E_g)^{1/2}$, where $h\nu$ is the photon energy, E_g is the bandgap and A_0 is a parameter associated with the transition probability. The absorption coefficient α is obtained by using the relation $\alpha = -(1/d) \ln(T)$, where T is the transmittance and d is the thickness of the film. Fig. 5 shows the plots of $(\alpha h\nu)^2$ vs. $h\nu$ of the ZnO films before and after ion irradiation. Band gap narrowing is observed in the ion irradiated samples, which can be attributed to lattice disorder, defect creation and a higher carrier concentration.

Magnetic and transport measurements were performed on the ZnO thin films at the different stages of processing. The diamagnetic contribution of the sapphire substrate, as denoted by the slope of the data at high fields, has been subtracted from the magnetization data. The ZnO films grown at 550°C and under a low oxygen partial pressure of 10^{-5} Torr show room temperature ferromagnetism with a saturation moment (M_S) of $\sim 1.7 \text{ emu cm}^{-3}$ and coercivity (H_C) of $\sim 150 \text{ Oe}$. Following the oxygen anneal at 700°C for 1 h they became non-magnetic, as shown in Fig. 6a. The free carrier concentration of as-grown films is $\sim 10^{19} \text{ cm}^{-3}$, whereas the oxygen annealed films show a concentration of $\sim 10^{15} \text{ cm}^{-3}$. Ferromagnetic ordering can be restored to the non-magnetic ZnO films by using either swift heavy ion irradiation or vacuum annealing, as seen in Fig. 6a and b, respectively. It is important to point out here that the same sample was used in both the oxygen anneal-

ing and ion irradiation experiments. The film which has been irradiated with a higher dose (10^{13} ions cm^{-2}) shows slightly higher saturation moments and coercivity. Ion irradiation at a 10^{13} cm^{-2} dose also results in an increase in the carrier concentration from $\sim 10^{15}$ to $\sim 10^{17}$ and a decrease in resistivity from $\sim 870 \Omega \text{ cm}$ to $\sim 6 \Omega \text{ cm}$. This is attributed to the incorporation of the shallow donor level induced by a $\text{V}_{\text{O}}\text{--I}_{\text{Zn}}$ defect complex [18]. In comparison to ion irradiation processing, previously reported laser irradiation treatments using a UV excimer laser had a much greater effect on the electrical properties, e.g. reaching carrier concentrations of $\sim 10^{19} \text{ cm}^{-3}$ after exposure to a few laser pulses [7]. Saturation magnetization and coercivity showed similar trends, i.e. both increased with an increase in ion dose or number of laser pulses, at least up to fairly large doses. Ferromagnetism can also be obtained by vacuum annealing of the non-magnetic (oxygen annealed) ZnO films. Fig. 6b shows the room temperature hysteresis loops of the ZnO film which was first annealed in oxygen and then in vacuum to introduce ferromagnetism. It can be seen that vacuum annealing for longer time results in higher M_S and H_C . The primary effect of vacuum annealing would be the creation of oxygen and zinc vacancies and interstitials; longer annealing times at high temperature (800°C) would lead to higher concentrations of these defects in the bulk film, which leads to enhanced ferromagnetism. Carrier concentration also increases by almost one order of magnitude when the annealing time is increased to 8 h.

In our experience, the onset of ferromagnetism in ZnO films, be it by laser irradiation, ion irradiation or vacuum annealing treatments, is always accompanied by n-type conductivity. However, no direct linear correlation between free carrier concentration and saturation moments seems to exist. For example, we have observed a strong temperature dependence of free carrier concentration in undoped ZnO films, but find that the M_S remains relatively temperature independent over the temperature range of $10\text{--}300 \text{ K}$ [8]. Similarly doping with up to 5% Al (n type) does not significantly affect the ferromagnetism, even though it increases the carrier densities by more than three orders of magnitude, rising from 1×10^{17} to $1.5 \times 10^{20} \text{ cm}^{-3}$ [19]. This lack of direct correlation between delocalized free carriers and saturation moments suggests that ferromagnetism does not arise from an itinerant mechanism in these undoped systems. Rather, the present study strongly suggests the existence of a direct correlation between the presence of defects in the ZnO, most likely oxygen vacancies and their complexes and ferromagnetism.

We propose that ion and laser irradiation introduces a large concentration of vacancy and interstitial defects in zinc and oxygen sublattices that explain both the n-type conductivity and ferromagnetism. Zinc vacancies are deep acceptors and give rise to very little p-type conductivity. The oxygen interstitials, which can have low migration energy depending upon their lattice location (tetrahedral

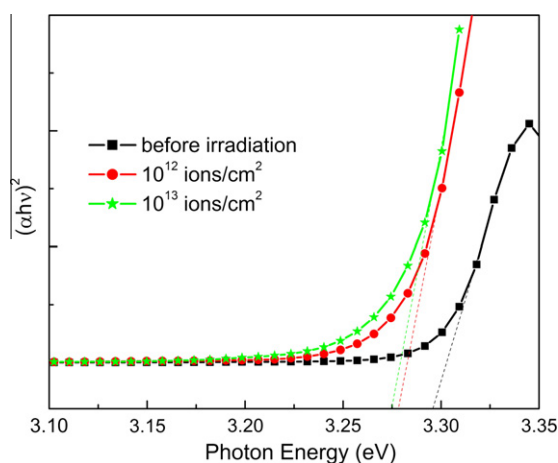


Fig. 5. Plots of $(\alpha h\nu)^2$ vs. $h\nu$ for the oxygen annealed (before irradiation) and ion irradiated films.

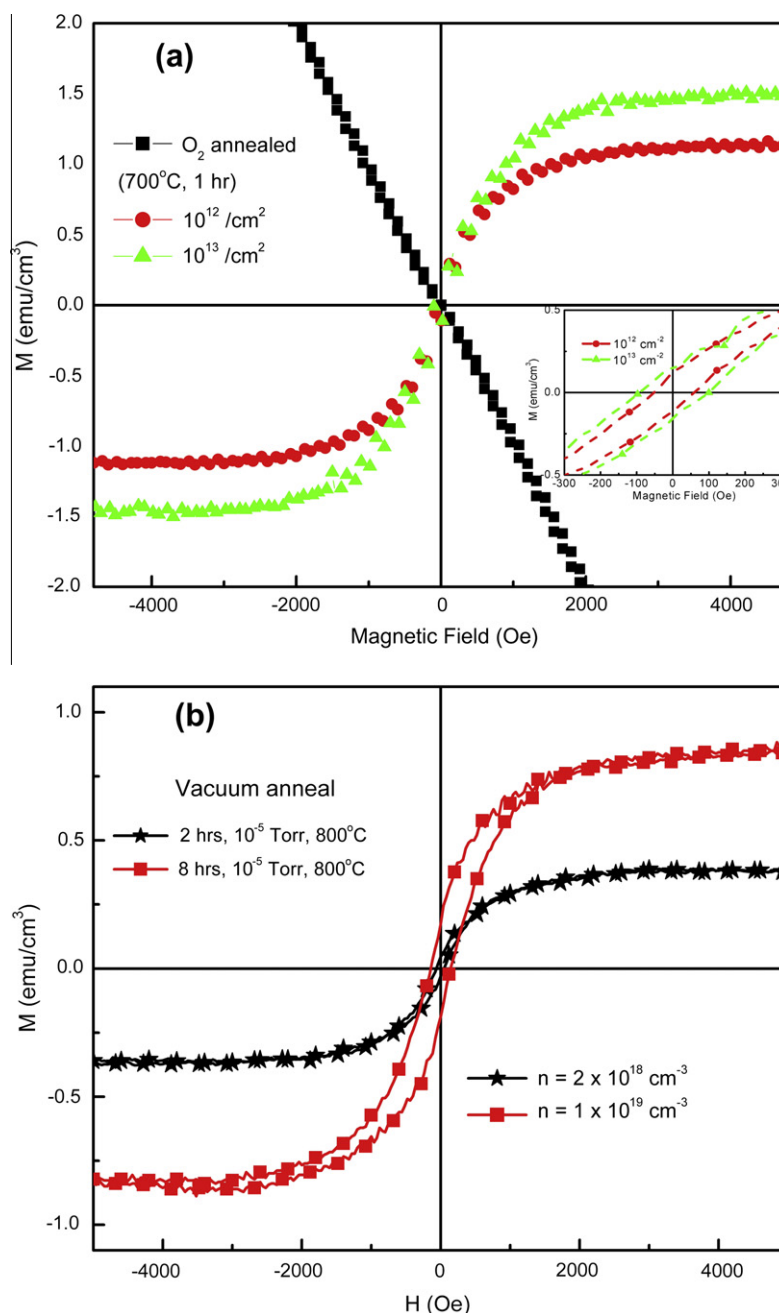


Fig. 6. (a) Room temperature M–H hysteresis curves of ZnO films annealed in oxygen and 300 MeV ¹⁰⁷Ag⁹⁺-irradiated at 10¹² and 10¹³ ions cm⁻² dose. (b) M–H hysteresis loops of ZnO films annealed in vacuum (10⁻⁵ Torr, 800 °C) for different times.

or octahedral sites), are expected to anneal out quickly. We postulate that the V_O–I_{Zn} defect complexes are the source of the observed n-type conductivity, consistent with the prediction by Kim and Park from their ab initio calculations [18]. Zinc interstitials are reported to have low migration energy, ~0.5 eV [20] and therefore are able to diffuse rapidly in the matrix and pair up quickly with oxygen vacancies to form shallow donor states that lead to n-type conductivity [20]. We believe that defects can also explain the existence of ferromagnetism. It is reported that unpaired 2p electrons at the O-sites surrounding a zinc

vacancy will introduce a magnetic moment on the order of 0.5 μ_B [9]. A bound magnetic polaron (BMP) then provides for long-range exchange coupling of the magnetic moments that result in ferromagnetism. This BMP arises from charged oxygen vacancies or V_O–I_{Zn} defect complexes that trap carriers (electrons) and have the potential to adopt a triplet ground state configuration that can couple nearby magnetic moments and produce room temperature magnetic ordering [21]. Prior EPR measurements having a broad peak at g = 2.01 [8] are consistent with this explanation. This is consistent with the presence of oxygen

vacancies ($g = 1.996$), and Zn vacancies ($g = 2.013$). In our model, annealing the samples in oxygen atmosphere definitely reduces the population of oxygen vacancies, destroying long-range magnetic order. Since our samples continue to show the n-type conductivity after vacuum annealing, we also envisage that the vacuum annealing creates V_O-I_{Zn} complexes that act as a source of the n-type conductivity and introduces zinc and oxygen vacancies (V_{Zn}) that result in ferromagnetism.

4. Conclusions

In summary, we have shown that ZnO films exposed to swift heavy ion irradiation with ^{107}Ag ions alters the optical, electrical and magnetic properties of the films without any significant change in the crystal structure. In particular, we report the onset of room temperature ferromagnetism in the insulating, non-magnetic ZnO films following swift heavy ion irradiation. The process introduces large amounts of lattice disorder and non-equilibrium point defects as a result of the electron–photon interactions and bond breaking that occurs during the irradiation process. Raman measurements revealed the appearance of two forbidden modes B_1^{low} and B_1^{high} upon irradiation due to relaxation of Raman selection rules associated with the breakdown of translational crystal symmetry. The observed changes in the E_2^{high} , E_2^{low} and $A_1(\text{LO})$ Raman modes are consistent with the creation of defects, vacancies and interstitials in zinc and oxygen sublattices. These results establish a strong correlation between RTFM and the presence of non-equilibrium concentrations of radiation induced defects, which are effective in generating some degree of 3-D ferromagnetic ordering. We propose a mechanism to explain RTFM and n-type conductivity in ZnO. We conclude that the n-type conductivity is derived primarily from oxygen vacancy–zinc interstitial (V_O-I_{Zn}) complexes. Likewise, zinc vacancies (V_{Zn}) give rise to the magnetic moment with oxygen vacancies forming bound magnetic polarons that couple these magnetic moments and finally lead to long-range ferromagnetism.

Acknowledgments

The authors are pleased to acknowledge the support of the Army Research Office under Grant W911NF-04-D-0003, and the National Science Foundation.

References

- [1] Panigrahy B, Aslam M, Misra DS, Ghosh M, Bahadur D. *Adv Funct Mater* 2010;20:1161.
- [2] Kapilashrami M, Xu J, Strom V, Rao KV, Belova L. *Appl Phys Lett* 2009;95:033104.
- [3] Xing G, Wang D, Yi J, Yang L, Gao M, He M, et al. *Appl Phys Lett* 2010;96:112511.
- [4] Venkatesan M, Fitzgerald CB, Coey JMD. *Nature (London)* 2004;430:630.
- [5] Hong NH, Sakai J, Poirot N, Brizé V. *Phys Rev B* 2006;73:132404.
- [6] Potzger K, Zhou S, Grenzer J, Helm M, Fassbender J. *Appl Phys Lett* 2008;92:182504.
- [7] Mal S, Narayan J, Nori S, Prater JT, Kumar D. *Solid State Commun* 2010;150:1660.
- [8] Mal S, Nori S, Jin C, Narayan J, Nellutla S, Smirnov AI, et al. *J Appl Phys* 2010;108:073510.
- [9] Wang Q, Sun Q, Chen G, Kawazoe Y, Jena P. *Phys Rev B* 2008;77:205411.
- [10] Van de Walle CG. *Phys Rev Lett* 2000;85:1012.
- [11] Janotti A, Wei SH, Zhang SB. *Appl Phys Lett* 2003;83:3522.
- [12] Ziegler JF. The stopping and range of ions in matter. <<http://srim.org/SRIM/SRIMLEGL.htm>>.
- [13] Szenes G. *Phys Rev B* 1995;51:8026.
- [14] Avasthi DK, Assmann W, Nolte H, Mieskes HD, Ghosh S, Mishra NC. *Nucl Instrum Methods: Phys Res Sect B* 2000;166–167:345.
- [15] Balamurugan B, Mehta BR, Avasthi DK, Singh F, Arora AK, Rajalakshmi M, et al. *J Appl Phys* 2002;92:3304.
- [16] Arguello CA, Rousseau DL, Porto SPS. *Phys Rev* 1969;181:1351.
- [17] Serrano J, Romero AH, Manjón FJ, Lauck R, Cardona M, Rubio A. *Phys Rev B* 2004;69:094306.
- [18] Kim YS, Park CH. *Phys Rev Lett* 2009;102:086403.
- [19] Chakarborty D, Trichy G, Narayan J, Prater JT, Kumar D. *J Appl Phys* 2007;102:113908.
- [20] Janotti A, Van de Walle CG. *Phys Rev B* 2007;76:165202.
- [21] Kittilstved KR, Schwartz DA, Tuan AC, Heald SM, Chambers SA, Gamelin DR. *Phys Rev Lett* 2006;97:037203.